Available online at www.sciencedirect.com
SCIENCE DIRECT®
Journal of Power Sources 141 (2005) 129–142
JOURNAL OF POWER SOURCES
www.elsevier.com/locate/jpowsour

Effect of $AlPO_4$-coating on cathodic behaviour of $Li(Ni_{0.8}Co_{0.2})O_2$

K.S. Tan, M.V. Reddy, G.V. Subba Rao, B.V.R. Chowdari*

Department of Physics, National University of Singapore, Singapore 117542, Singapore

Received 7 July 2004; accepted 31 August 2004
Available online 27 October 2004

Abstract

The cathodic behaviour and thermal stability in the charged state of bare and 1–8 wt.% $AlPO_4$-coated layered oxide $Li(Ni_{0.8}Co_{0.2})O_2$ are investigated. The synthesized compounds are characterized by a wide variety of techniques. X-ray diffraction analysis (XRD) shows that the hexagonal *a* and *c* lattice parameters of $Li(Ni_{0.8}Co_{0.2})O_2$ are not affected by the $AlPO_4$-coating, but there are indications of an increasing number of Ni-ions occupying the Li-sites in the Li-layer with increasing amounts of the coated $AlPO_4$. The O 1s X-ray photoelectron spectra clearly indicate two different oxygens that correspond to the coated-$AlPO_4$ and the bare compounds. Cyclic voltammetry (2.5–4.3 V) shows that the characteristic structural phase transitions exhibited by the bare compound are suppressed by $\geq$5 wt.% $AlPO_4$-coating. Galvanostatic charge–discharge cycling has been carried out at a current density of 30 mA g^{-1} in the range of 2.5–4.3 V up to 70 cycles and 2.5–4.5 V up to 40 cycles. Capacity-fading of the 3 and 5 wt.% $AlPO_4$-coated $Li(Ni_{0.8}Co_{0.2})O_2$ is much less than that shown by the bare compound, which is 21% between 10 and 70 cycles with a 4.3 V cut-off and 48% between 10 and 40 cycles with a 4.5 V cut-off. The coulombic efficiency is >98% in all cases after a few initial cycles. Impedance spectra of cells with 1 and 5 wt.% $AlPO_4$-coated compounds and ex situ XRD of the 3 and 5 wt.% $AlPO_4$-coated charged cathodes are examined and the results interpreted. Differential scanning calorimetry curves of the charged cathodes (4.3 V) reveals that the decomposition temperature of 220 °C for the bare compound is increased by ~10 °C after 3 and 5 wt.% $AlPO_4$-coating, and more significantly the heat evolution decreases by a factor of 5, which indicates better thermal stability. Nevertheless, this benefit comes at the expense of reversible capacities, which decrease from 202 mAh g^{-1} (fifth cycle, 4.3 V) for the bare compound, to 156 and 100 mAh g^{-1} for the 3 and 5 wt.% $AlPO_4$-coated $Li(Ni_{0.8}Co_{0.2})O_2$, respectively.

Keywords: $Li(Ni_{0.8}Co_{0.2})O_2$; $AlPO_4$-coating; Cathode; Li-ion batteries; Thermal stability

1. Introduction

The ever-increasing demand for portable telecommunication devices, computers and eventually, hybrid vehicles has given rise to the increased production of Li-ion rechargeable batteries to provide the required power sources [1–3]. Since Li-ion batteries (LIBs) surpass all the rechargeable batteries available in the market by having the highest energy density per weight or volume, they are considered to be the most suitable dc power sources. At present, $LiCoO_2$ is commonly used as the cathode (positive) material in LIBs because of its high volumetric energy density, excellent cycleability and the ease at which it is synthesized from raw materials. On the other hand, $LiCoO_2$ does have three major disadvantages, namely, the high material cost, toxicity and only 50% utilization of the theoretical capacity. This has resulted in the search for alternative cathode materials with better electrochemical performance and lower cost. Nickel (Ni) and manganese (Mn) containing compounds of the type, $LiNiO_2$ [4,5], $Li(Ni_{1/2}Mn_{1/2})O_2$ [6–8] and $LiMn_2O_4$ [9] and their doped derivatives have been studied extensively.

Over the years, the composition $Li(Ni_{0.8}Co_{0.2})O_2$ (along with minor variations in the Ni:Co ratio) has attracted much attention as a 4 V cathode due to its many advantages compared with $LiCoO_2$ [10–30], viz., (i) It contains only 20 at.% of toxic cobalt and is cheaper than $LiCoO_2$; (ii) it can be synthesized from raw materials at a lower temperature

* Corresponding author. Tel.: +65 6874 2956; fax: +65 6777 6126.
E-mail address: phychowd@nus.edu.sg (B.V.R. Chowdari).

0378-7753/$ – see front matter © 2004 Elsevier B.V. All rights reserved.
doi:10.1016/j.jpowsour.2004.08.044

(700–800 °C) than $LiCoO_2$, but heating in an oxygen atmosphere is preferred; (iii) it can give a higher reversible capacity in the voltage range 2.5–4.3 V versus Li/Li^+ compared with $LiCoO_2$, since the electroactive species involved are Ni^{3+} ions. Studies have shown, however, that $Li(Ni_{0.8}Co_{0.2})O_2$ possesses some disadvantages and needs to be optimized before it can be employed in practical LIBs.

The compound exhibits crystal structure phase transitions, similar to $LiNiO_2$, during the charging process due to the de-insertion of Li-ions (increase of x in $Li_{1-x}(Ni_{0.8}Co_{0.2})O_2$). These are reversible and hence during charge–discharge cycling, minor changes in the unit-cell volume produces 'electrochemical grinding' that results in capacity-fading. This can be reduced to some extent by optimizing the synthesis procedure, by doping with other elements at the Co-sites, or by coating the surface of the particles with other oxides/compounds. In the charged state, i.e., at $x > 0.5$ in $Li_{1-x}(Ni_{0.8}Co_{0.2})O_2$, the compound is a strong oxidizing agent due to the presence of Ni^{4+} ions and can slowly cause the decomposition of the liquid electrolyte that results in the evolution of gases. In addition, for $x > 0.5$, the compound is structurally unstable when heated above 200 °C and evolves oxygen and decomposition products. Thus, there is every likelihood of a violent reaction and explosion in case of accidental heating and/or short-circuiting of a charged LIB using this material. Doping at the Co-sites [28] as well as surface-coating of $Li(Ni_{0.8}Co_{0.2})O_2$ by MgO [31], TiO_2 [32–34], SiO_x [35] are some of the strategies employed to reduce or completely suppress the above effects.

Recently, Cho and co-workers [36–40] reported that surface-coating of $LiCoO_2$ particles with a layer of aluminum phosphate ($AlPO_4$) dramatically reduces the heat evolution of the electrode in the charged state. They have also shown that an LIB fabricated with $AlPO_4$-coated $LiCoO_2$ as the cathode and a graphite anode exhibits excellent thermal stability in the over-charged (12 V) state, and also passes many other safety tests. In the study reported here, bare and $AlPO_4$-coated $Li(Ni_{0.8}Co_{0.2})O_2$, have been prepared and their electrochemical properties and thermal stability have been examined in the charged state.

2. Experimental

Bare $Li(Ni_{0.8}Co_{0.2})O_2$ was prepared by the solid-state reaction method. High purity LiOH (Merck) and commercially available $(Ni_{0.8}Co_{0.2})(OH)_2$ powder were weighed in stoichiometric ratio to give 20 g product and then mixed in an auto-grinder. The mixture was packed tightly in an alumina boat and heated in a programmable tubular furnace (Carbolite, UK) fitted with oxygen gas flow. The furnace was heated at a rate of 3 °C min^{-1} until the temperature reached 725 °C. The heating was continued for 20 h at this temperature and the furnace was then shut off but the O_2 flow was continued. After cooling to room temperature, the product was ground to fine powder.

For the nominal 3 wt.% coating of $AlPO_4$ on to the particles of the cathode material, the procedure of Cho et al. [37–39] was followed, namely, 0.162 g of $(NH_4)_2HPO_4$ (Merck) and 0.461 g of $Al(NO_3)_3{\cdot}9H_2O$ (Merck) were weighed and separately dissolved in distilled water to form colourless solutions of 1:1 mol concentration. The two solutions were then mixed and stirred to produce a white suspension into which 5 g of $Li(Ni_{0.8}Co_{0.2})O_2$ powder was added. The mixture was stirred for 3 h and transferred to a Petridish and heated on a hot plate at 60 °C to drive off most of the water. When the mixture had became a thick slurry, it was transferred to an oven for drying at 100 °C for 24 h. The dried compound was recovered and ground to ensure proper mixing, packed into an alumina boat and sintered in the tubular furnace in an oxygen atmosphere at 700 °C for 5 h. The product was allowed to cool to room temperature in an oxygen flow and reground. This process was repeated for the 5, 8 and 10 wt.% of $AlPO_4$-coating with appropriate weights of the starting materials.

Characterization of the bare and $AlPO_4$-coated compounds was carried out by powder X-ray diffraction (XRD) (Philips PW1820/00 Vertical Goniometer; Cu Kα radiation) to identify the crystal structure. The unit-cell lattice parameters were obtained by the least-squares fitting of all the peak positions (2θ range, 10–70°) in the XRD patterns. The morphology of the powders was examined by means of a scanning electron microscope (SEM) (JEOL JSM-6700F). High resolution transmission electron microscopy was carried out with a JEOL 3010 instrument. Back-scattered electron images were obtained with a JEOL JSM-5310LV instrument. The Brunauer, Emmett and Teller (BET) surface area of the powder was measured with Micromeritics Tristar 3000 (USA) equipment and density determination was undertaken with an AccuPyc 1330 pycnometer (Micromeritics, USA). X-ray photoelectron spectra of the compounds were obtained using a VG Scientific ESCA MK II spectrometer with monochromatic Mg Kα radiation (1253.6 eV). The survey spectra were obtained in the range 0–1099 eV (constant-pass energy = 50 eV), and the high resolution spectra were recorded with a constant pass energy mode of 20 eV. Charge referencing was carried out against adventitious carbon C (C 1s binding energy = 284.6 eV). Analysis of the XPS spectra was performed with XPS Peak-fit software. A Shirley-type background was subtracted from the recorded spectra and curve-fitting was carried out with a Gaussian–Lorentzian (ratio 60:40) curve. The derived binding energies (BE) were accurate to ±0.1 eV.

The cathodes for electrochemical studies were fabricated from a mixture of the following composition: active material, super P carbon black (electronically conducting additive) and polymer binder (Kynar 2801) in the weight ratio 70:15:15, as described elsewhere [8,32,41]. *N*-Methyl-pyrrolidone (NMP) was used as the solvent for the mixture, which was stirred to form a homogeneous and viscous slurry. The slurry was then cast on to an etched Al-foil (15 μm thick, Alpha Industries Co. Ltd., Japan) to form a thick layer (22–23 μm) by the

doctor-blade method. The film was dried at 80 °C for 12 h in an air oven, smoothed by pressing through stainless-steel twinrollers and then cut into circular discs (16 mm diameter). The discs were vacuum dried at 70 °C for 12 h, cooled and transferred into an argon-filled glove-box (MBraun, Germany) for cell assembly. The atmosphere in the glove-box was maintained at <1 ppm of H_2O and O_2. The weight of the active material was deduced from the total weight of the disc (Al foil, sample powder, carbon black and binder).

For coin-cell (size 2016) assembly, a Celgard 2502 membrane was used as the separator and the electrolyte was 1 M $LiPF_6$ in ethylene carbonate (EC) + diethyl carbonate (DEC) in the ratio of 1:1 by volume (Merck, Selectipur LP40). The Li-metal anode was obtained from Kyokuto Metal Co., Japan, and was cut into circular discs (16 mm diameter). Cyclic voltammetry and galvanostatic cycling tests were conducted at room temperature (25 °C) using a potentiostat/galvanostat system (Mac-pile II, Bio-logic, France) and a Bitrode multiple battery tester (Model SCN, Bitrode, USA). The cells were aged for 24 h before testing.

Differential scanning calorimetry (DSC; TA Instruments, Model 2920, USA) was used to study the thermal stability of charged cathodes. For this purpose, the respective cell was charged to 4.3 V at 30 mA g^{-1} after selected cycles and held at that voltage for 2 h. The cell was then dismantled in the glove-box to recover the charged cathode, which was then washed with DEC, dried and packed into an Al-cup. The cathodes were also subjected to ex situ XRD phase analysis. A computer-controlled Solatron impedance/gain-phase analyzer (model SI 1255) coupled with a battery test unit (model 1470) was used for impedance measurements on the cells at room temperature. The frequency range was from 0.35 MHz to 3 mHz with an ac signal amplitude of 5 mV. The resulting data were analyzed by using Zplot and Z view software (Version 2.2, Scribner associates Inc., USA) to obtain the Nyquist plots.

3. Results and discussion

3.1. Structure and morphology

Bare (uncoated) and $AlPO_4$-coated $Li(Ni_{0.8}{}^{3+}Co_{0.2}{}^{3+})O_2$ compounds are black crystalline powders. The XRD patterns of these compounds, which are indexed on the basis of hexagonal O3-structure of $LiCoO_2$ with the space group $R\bar{3}m$, are presented in Fig. 1. The least-squares fitted lattice parameters, calculated from *d*-spacings and Miller indices are given in Table 1. For the bare-compound, the XRD pattern and the hexagonal *a* and *c* parameters agree well with those reported in the literature [11,14,15,21,27]. The *c*:*a* ratio of 4.94 and the well-defined splitting of the peaks assigned to the pairs of Miller indices (0 0 6, 1 0 2) and (1 0 8, 1 1 0) are both a good indication of a well-ordered layer structure (Fig. 1). On the other hand, the relative intensity ratio (*R*) of the (0 0 3) and (1 0 4) lines in the XRD pattern is 1.02 for the bare compound

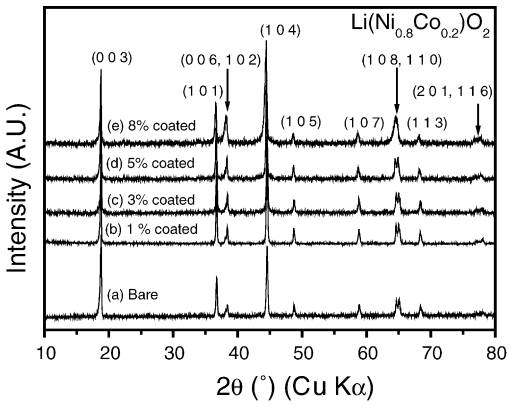

Fig. 1. XRD patterns of bare and $AlPO_4$-coated $Li(Ni_{0.8}Co_{0.2})O_2$: (a) bare; (b)–(e) 1, 3, 5, 8 wt.% $AlPO_4$-coated compounds. Cu Kα radiation. Miller indices (*h k l*) are shown.

and this indicates the presence of a small numbers of Ni-ions at the Li-sites in the Li-layer.

The XRD patterns of $AlPO_4$-coated $Li(Ni_{0.8}Co_{0.2})O_2$ display a slight broadening of the major peaks but there is essentially no change in the *a* and *c* lattice parameters (Fig. 1 and Table 1). This indicates that, as a stable compound, $AlPO_4$ not being doped into $Li(Ni_{0.8}Co_{0.2})O_2$ and only forms a surface-layer after heat-treatment at 700 °C. The 8 wt.% $AlPO_4$-coated compound shows small-intensity lines due to $AlPO_4$ in the 2θ range, 20–25° and near to 34° (Fig. 1(e)). Indeed, the 10% $AlPO_4$-coated compound displays clearly the peaks due to $AlPO_4$ in the XRD pattern (not shown in Fig. 1). It is noted however, that the (0 0 6, 1 0 2) and (1 0 8, 1 1 0) doublet-peaks have merged and the other major lines in the XRD pattern have further broadened in the 8 wt.% $AlPO_4$-coated compound. Also, while the *c*:*a* ratio remains almost unchanged (4.93 ± 0.02), the *R* value shows a decreasing trend with an increase in the $AlPO_4$-content and reaches 0.73 in the 8 wt.% $AlPO_4$-coated compound (Table 1). This shows significant amounts of Ni-ions in the Li-layer compared with bare $Li(Ni_{0.8}Co_{0.2})O_2$. It must be mentioned, however, that a small number of Al-ions from $AlPO_4$ may become doped into the surface layers of the bare compound during heat treatment. Since the ionic radii of Co^{3+} (0.545 Å, low spin) and Al^{3+} (0.535 Å) are almost the same for octahedral oxygen coordination [42], minor changes in the *a* and *c* values are not observed for $AlPO_4$-coatings of 1–8 wt.%.

Electron micrographs (SEM) for the bare and the $AlPO_4$-coated $Li(Ni_{0.8}Co_{0.2})O_2$ are presented in Fig. 2. An agglomeration of sub-micron particles of $Li(Ni_{0.8}Co_{0.2})O_2$ with platelet morphology are clearly seen in all the samples. The presence of crystalline nano-sized $AlPO_4$ particles on the surface of the host material is evident in Fig. 2(c) and (d). The electron micrographs and the corresponding back-scattered electron (BSE) image of the 8 wt.% coated compound are given in Fig. 3 at a lower magnification (10 μm). The white spheres in the BSE image (Fig. 3(b)) represent the host oxide

Table 1
Hexagonal lattice parameters and relative intensity ratio (R) of (0 0 3) and (1 0 4) reflections for bare and $AlPO_4$-coated $Li(Ni_{0.8}Co_{0.2})O_2$

x wt.% $AlPO_4$-coated $Li(Ni_{0.8}Co_{0.2})O_2$	a (Å, ±0.008)	c (Å, ±0.02)	c:a	$R = I_{003}/I_{104}$
$x = 0$ (bare)	2.867	14.17	4.94	1.02
$x = 1$	2.868	14.17	4.94	0.97
$x = 3$	2.871	14.16	4.93	0.80
$x = 5$	2.875	14.20	4.94	0.85
$x = 8$	2.879	14.19	4.95	0.73
$x = 3$, after 25 cycles, 2.5–4.3 V; discharged state	2.872	14.18	4.93	1.2
$x = 3$, after 70 cycles, 2.5–4.3 V; charged state	2.853	14.25	4.99	0.60
$x = 5$, after 70 cycles, 2.5–4.3 V; charged state	2.839	14.39	4.99	0.62
$x = 8$, after 40 cycles, 2.5–4.3 V; charged state	2.832	14.44	5.09	0.67

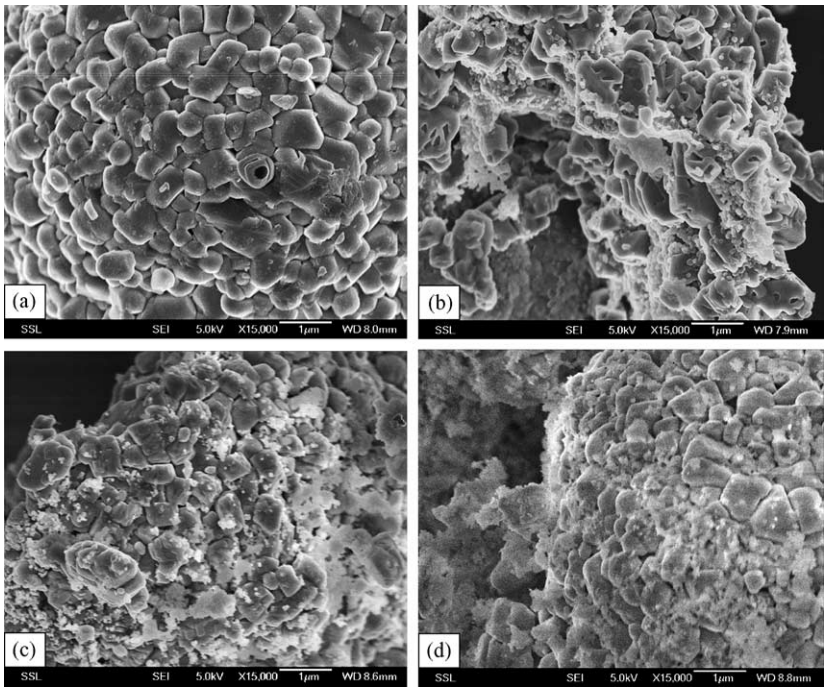

Fig. 2. Scanning electron micrograph of (a) bare, (b) 3 wt.%, (c) 5 wt.% and (d) 8 wt.% $AlPO_4$-coated $Li(Ni_{0.8}Co_{0.2})O_2$. Bar scale, 1 μm.

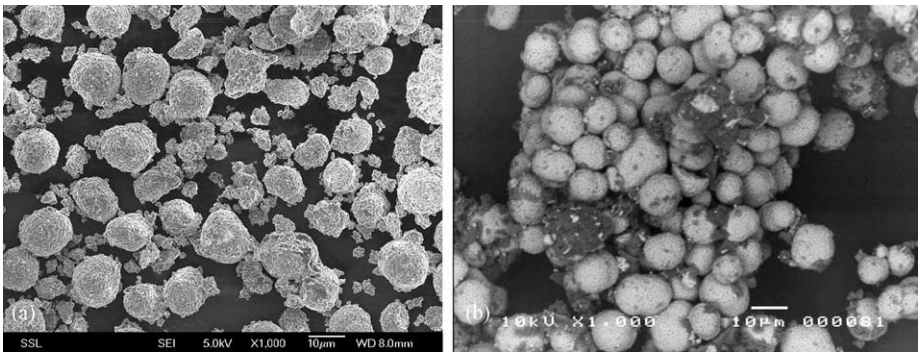

Fig. 3. (a) Scanning electron micrographs and (b) back scattered electron (BSE) image of 8 wt.% $AlPO_4$-coated $Li(Ni_{0.8}Co_{0.2})O_2$. Bar scale, 10 μm.

particles whereas the dark patches are the $AlPO_4$ particles. Using energy dispersive spectroscopy (EDS), the elemental composition (Al, P, Ni, Co, O) was found to be consistent with the expected distribution. From the data in Figs. 2 and 3, it is clear that $AlPO_4$ is not coated uniformly on $Li(Ni_{0.8}Co_{0.2})O_2$ for concentrations $\geq$5 wt.%.

Fig. 4 shows the HRTEM photographs of bare and 5 wt.% $AlPO_4$-coated $Li(Ni_{0.8}Co_{0.2})O_2$. The crystal edges of the coated particle appear wavy and translucent in comparison with those of the bare compound. The interface between the coating and the cathode substrate is indicated by an arrow in Fig. 4(b). The $AlPO_4$ nano particles that have crystallized on the surface of the coating are indicated as A_1 and A_2. The BET surface areas are 0.14 and $1.32 \pm 0.02\ m^2 g^{-1}$ for the bare and 3 wt.% $AlPO_4$-coated compound, respectively. This shows that coating results in a 10-fold increase in the surface area of the particle. The measured density of the bare $Li(Ni_{0.8}Co_{0.2})O_2$ powder was $4.74\ g\ cm^{-3}$ and compares well with the calculated X-ray density of $4.82\ g\ cm^{-3}$.

3.2. XPS spectra

X-ray photoelectron spectroscopy (XPS) is a well-adapted, non-destructive technique for the evaluation of valence states of the metal/non-metal ions in solids [43], and is extensively used in the characterization of cathode materials [8,41,44–50]. The core level spectra for Li 1s and O 1s for the bare and 3 and 5 wt.% $AlPO_4$-coated $Li(Ni_{0.8}Co_{0.2})O_2$ are shown in Fig. 5. The binding energies (BE) are given in Table 2. The bare compound shows a single peak for O 1s with a BE of 531.8 eV that can be assigned to the oxygen that is predominantly bonded to Ni-ions in the lattice [41,44,47,48]. The $AlPO_4$-coated $Li(Ni_{0.8}Co_{0.2})O_2$ show unsymmetrical spectra in the 526–534 eV region and are fitted into two peaks that clearly indicate two different types of oxygen. The high-intensity peak at 531.4 ± 0.2 eV corresponds to that of the host compound, whereas that in the region 529–530 eV is O 1s due to $AlPO_4$. The relative intensity of this peak increases, as expected, in the 3 and 5 wt.% $AlPO_4$-coated compounds and indicate that the assignment is correct Fig. 5(a).The O 1s BEs of 529.2 and 530.0 eV for the 3 and 5 wt.% $AlPO_4$-coated compounds (Table 2) are, however, smaller than the value of 531.44 eV reported for bulk $AlPO_4$ [51].

The Li 1s peak in the bare and $AlPO_4$-coated compounds (Fig. 5(b)) shows a BE in the range 54.8–55.2 eV, which is in good agreement with values reported for similar oxide cathodes [8,41,44,48]. The XPS spectra of Ni, Al, and P for the 3 and 5 wt.% $AlPO_4$-coated compounds, are presented in Fig. 6. The BE values of Ni, Co, Al and P are given in Table 2. The Ni $2p_{3/2}$ shows BEs in the range of 855.3 ± 0.2 eV and these values are well matched with the BE of Ni^{3+} in $LiNiO_2$ [41,47,48]. The multiple splitting of the energy levels of Ni-ion gives rise to satellite peaks around 862 eV and these are observed in Fig. 6 [41]. The Co $2p_{3/2}$ spectra show a single peak with a BE in the range 780–781 eV for the bare and coated compounds (Table 2). These values agree well with those reported for Co^{3+} in $LiCoO_2$ [45] and $Li(Ni_{1/3}Co_{1/3}Mn_{1/3})O_2$ [41].

The Al 2p spectrum shows a characteristic BE of 73.3 eV and the relative peak intensity increases for the 3 and 5 wt.% coated compound (Fig. 6(b) and Table 2). This BE value is lower by 1.2 eV compared with Al (2p) in $AlPO_4$ [51]. The P 2p peak has a BE of 133.4 ± 0.1 eV in the coated compounds which is characteristic of the tetrahedral (PO_4)-group. The value is smaller than the 135.03 eV reported for P 2p in $AlPO_4$ [51]. Considerable increase in the peak area with increase of coating concentration occurs, as shown in Fig. 6(c). Thus, the XPS results indicate that the predominant oxidation states of Ni and Co are +3 in $Li(Ni_{0.8}Co_{0.2})O_2$. The corresponding BEs of Ni, Co and O are little affected by coating with $AlPO_4$ which suggests that Al or P are not incorporated into the crystal lattice during the coating process. The coated $AlPO_4$ is clearly identified by XPS. The observed BEs of O, Al and P are smaller, by 1–2 eV, in comparison with those reported for bulk $AlPO_4$. This shows that the BEs are modified by the nano-particle nature and/or are due to the effect of coating on to another host oxide.

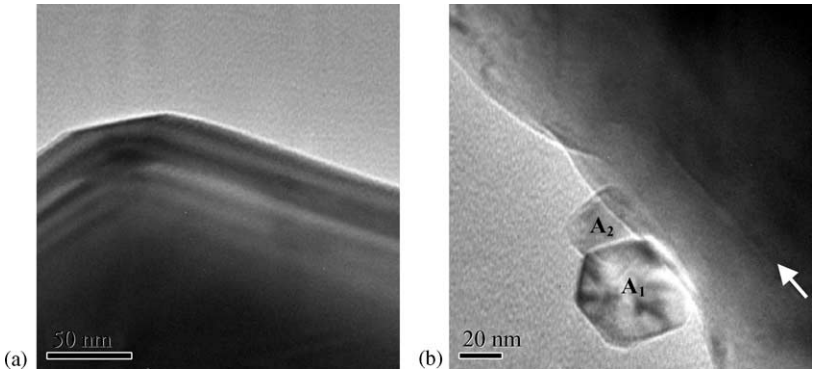

Fig. 4. HRTEM images of (a) bare $Li(Ni_{0.8}Co_{0.2})O_2$; bar scale, 50 nm. (b) 5 wt.% $AlPO_4$-coated $Li(Ni_{0.8}Co_{0.2})O_2$. Bar scale, 20 nm.

Table 2
Binding energies (±0.1 eV) of elements in bare and $AlPO_4$-coated $Li(Ni_{0.8}Co_{0.2})O_2$

$Li(Ni_{0.8}Co_{0.2})O_2$	Li (1s)	O (1s)	Ni^{2+} ($2p_{3/2}$)	Co^{3+} ($2p_{3/2}$)	Al (2p)	P (2p)
Bare	55.2	–; 531.8	855.5	781.1	–	–
3 wt.% coated	54.8	529.2; 531.2	855.4	780.2	73.3	133.4
5 wt.% coated	55.1	530.0; 531.6	855.2	781.1	73.3	133.5

3.3. Electrochemical properties

3.3.1. Cyclic voltammetry

Cyclic voltammetry is a complementary and well-suited technique to evaluate the cathodic performance and electrode kinetics of oxide materials [8,18,24,47,49]. The cyclic voltammograms (CV) of bare and $AlPO_4$-coated $Li(Ni_{0.8}Co_{0.2})O_2$ cathodes were recorded for the cells at room temperature with metallic lithium as the counter and reference electrodes in the range 2.5–4.3 V (or 4.5 V) at various scan rates. The CV at a scan rate of 0.058 mV s^{-1} up to 30 cycles are presented in Fig. 7. For clarity, only select cycles are shown. In the case of bare $Li(Ni_{0.8}Co_{0.2})O_2$, the first cycle anodic peak (extraction of Li ions from the lattice) occurs at 4.20 V (versus Li), whereas the main cathodic (insertion of Li) peak is at 3.68 V. A minor (shoulder) cathodic peak at 3.9 V is also seen in Fig. 7(a) and (e). In the second cycle, the anodic peak shifts to a lower voltage (3.76 V), but the corresponding cathodic peak shifts only slightly, by 0.02 V, to a higher voltage. The shift in the anodic peak voltage is an indication of the 'formation' of the electrode in the first cycle, whereby the active material makes good electrical contact with the conducting carbon particles in the composite electrode, liquid electrolyte and current-collector. The hysteresis (ΔV = the difference between the 10th anodic and cathodic peak voltages) is 0.02–0.03 V which indicates good reversibility of the charge–discharge reaction. Subsequent CVs show that ΔV remains almost constant, but the relative peak-intensities (and area under the peak) decrease with cycle number. This is due to capacity-fading. The major anodic/cathodic peaks at ~3.7 V are assigned to the $Ni^{3+/4+}$ redox couple. In this voltage region, the anodic peak also

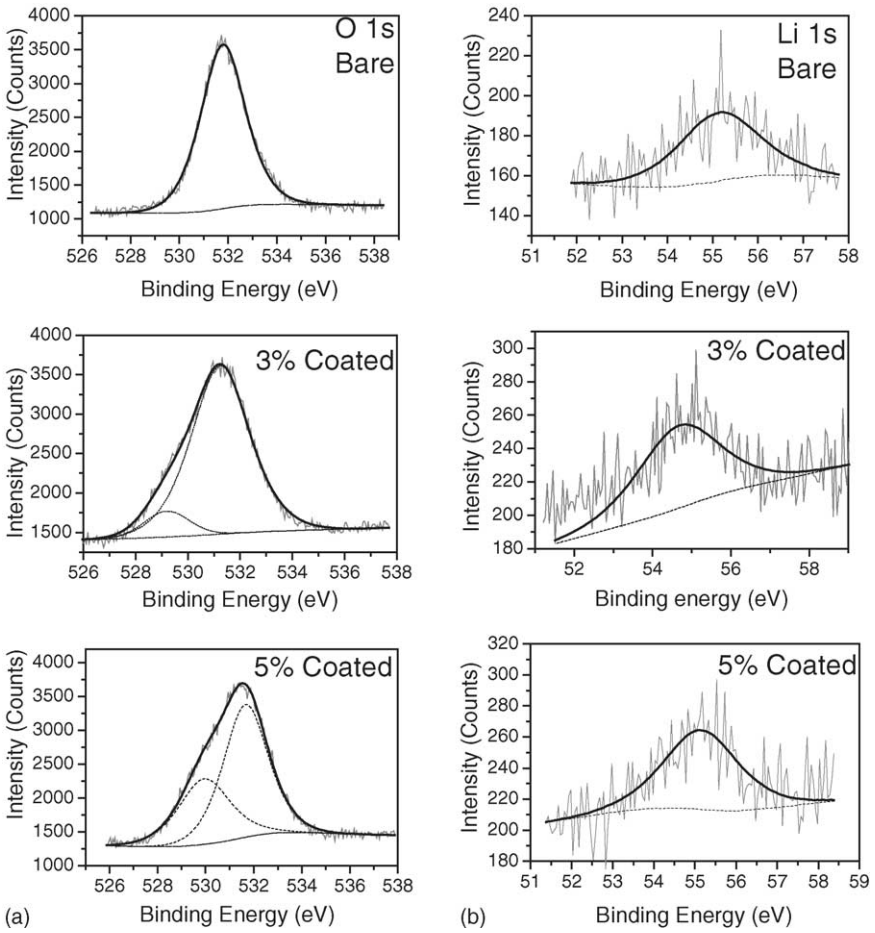

Fig. 5. XPS core level spectra of bare and $AlPO_4$-coated $Li(Ni_{0.8}Co_{0.2})O_2$: (a) O (1s); (b) Li (1s). Curve fitting of the peaks is shown. Dotted line represents Shirley-type background and thick line over raw data is the summation over fitted contributions.

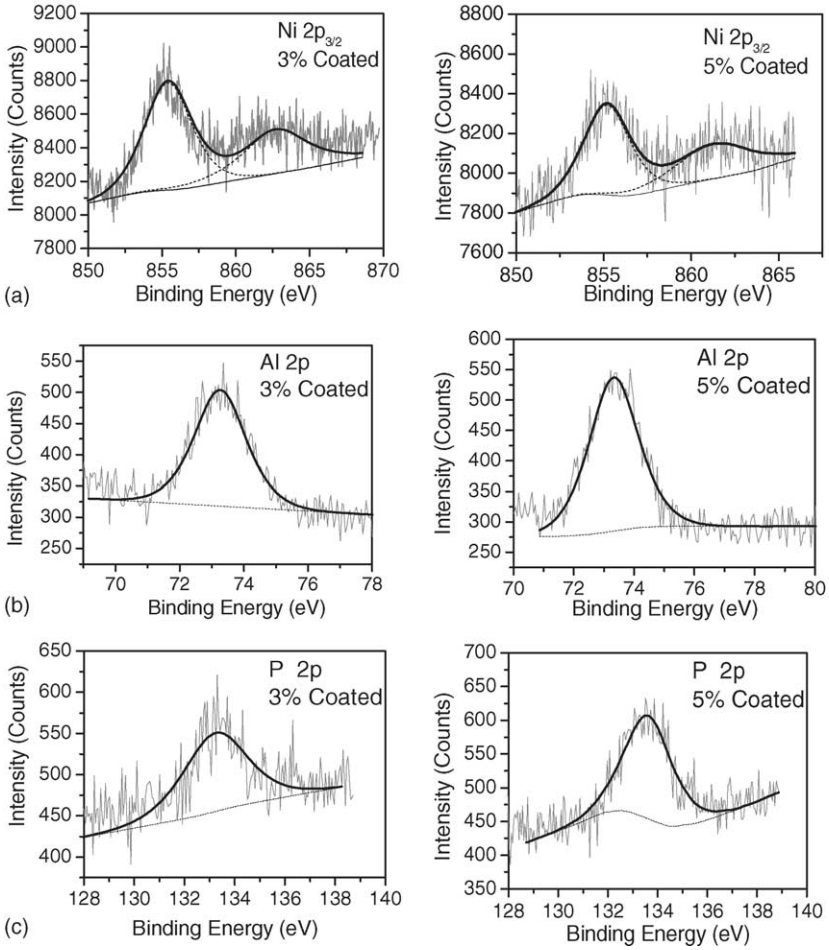

Fig. 6. XPS core level spectra of bare and $AlPO_4$-coated $Li(Ni_{0.8}Co_{0.2})O_2$: (a) Ni ($2p_{3/2}$); (b) Al (2p); (c) P (2p). Curve fitting of peaks is shown. Dotted line represents Shirley-type background and thick line over raw data is summation over fitted contributions.

has a shoulder during 5–10 cycles and this develops into a clear peak at ~3.75 V during 20–25 cycles Fig. 7(a). This is characteristic of the two-phase region corresponding to the hexagonal (H1) to monoclinic (M) phase transition in $Li(Ni_{0.8}Co_{0.2})O_2$ [18]. This peak is not, however, clearly delineated in the cathodic peak. The anodic/cathodic peaks in the CV at 4.01/3.95 and 4.2/4.15 V are assigned to the M-to-hexagonal (H2) and H2-to-hexagonal (H3) phase transitions, respectively [18,20,24,28,34]. It is known that these reversible phase transitions in $LiNiO_2$ [52] persist also in $Li(Ni_{0.8}Co_{0.2})O_2$ with a reduced intensity and are completely suppressed by Co-doping only at concentrations ≥30 at.% [18,53]. Thus, in our case, the CV data for the bare compound in the ranges 2.5–4.3 and 2.5–4.5 V show that these transitions occur at the relevant voltages with a reduced-intensity and are responsible for the observed capacity-fading.

The effect of $AlPO_4$-coating is clearly revealed in the CVs presented in Fig. 7(b–d) (2.5–4.3 V) and (f) (2.5–4.5 V). The 'formation' of the electrode in the first cycle is similar to that of the bare compound in all cases. The CV of 1 wt.% $AlPO_4$-coated $Li(Ni_{0.8}Co_{0.2})O_2$ is almost identical to that of the bare compound. For the 3 wt.% $AlPO_4$-coated compound, the main anodic/cathodic peaks in the CV that correspond to Li extraction/insertion (5–30 cycles) still occur in the voltage region, 3.6–3.8 V, but the H1↔M transition peak at ~3.75 V is suppressed and the relative intensities of the peaks due to H1 ↔ H2, and notably of the H2 ↔ H3 phase transitions, have decreased considerably, which indicates a suppression effect (Fig. 7(b)). Though the ΔV is decreased (e.g., to 0.07 V at the 10th cycle), the intensity of the main redox peaks also decreases during 10–30 cycles, which is indicative of some capacity-fading for this composition. For 5 and 8 wt.% $AlPO_4$-coated $Li(Ni_{0.8}Co_{0.2})O_2$, the CVs (2.5–4.3 V, 2–20 cycles) show that the H1 ↔ H2 and H2 ↔ H3 phase transitions have been completely suppressed, in addition to the H1 ↔ M transition, because there are no peaks in the corresponding voltage region. On the other hand, the ΔV values are increased considerably (e.g., 0.23 and 0.49 V, respectively for 5 and 8 wt.% coating at the 10th cycle; 2.5–4.3 V) and are due to electrode polarization. Also, there is some capacity-fading, as reflected in a decrease in the relative intensities of the main redox peaks (Fig. 7(c) and (d)). The CV of 5 wt.% $AlPO_4$-coated $Li(Ni_{0.8}Co_{0.2})O_2$ in the voltage range 2.5–4.5 V (Fig. 7(f)), however, resem-

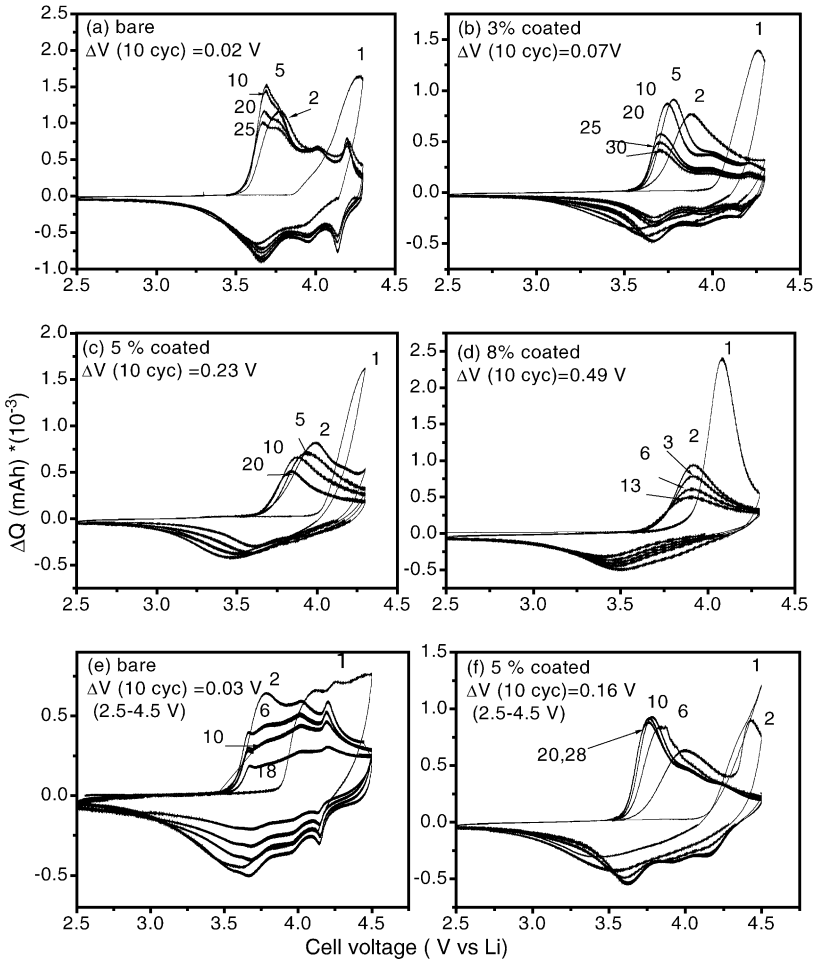

Fig. 7. Cyclic voltammograms of (a) bare and (b)–(d) 3, 5 and 8 wt.% $AlPO_4$-coated $Li(Ni_{0.8}Co_{0.2})O_2$ between 2.5 and 4.3 V; (e) bare and (f) 5 wt.% $AlPO_4$-coated $Li(Ni_{0.8}Co_{0.2})O_2$ between 2.5 and 4.5 V. Scan rate 0.058 mV s^{-1}. Numbers refer to cycle numbers.

bles that of the 3 wt.% coated-compound (range 2.5–4.3 V) rather than that of Fig. 7(c). The only difference is that $\Delta V = 0.16$ V, i.e., a value in between those shown by 3 and 5 wt.% coated-compounds. This indicates that the H1 ↔ H2 and H2 ↔ H3 transitions are not completely suppressed in the 5 wt.% $AlPO_4$-coated compound when the upper cut-off voltage is increased from 4.3 to 4.5 V.

The CVs were also recorded at various scan rates, from 0.058 to 0.40 mV s^{-1} for the bare and 5 wt.% $AlPO_4$-coated compound in the range 2.5–4.3 V. The data are given in Fig. 8. As expected, the ΔV values and the peak-current (i) increase with increase in the scan-rate, which is typical of intercalation electrodes such as $LiMn_2O_4$ [54,55] and $LiCoO_2$ [56] and is an indication of transition from a finite to a semi-infinite diffusion process of Li-ions within the crystal lattice. In the present case, however, the peak current, i, does not vary as the square root of the scan-rate, but appears to vary linearly and 5 wt.% $AlPO_4$-coated $Li(Ni_{0.8}Co_{0.2})O_2$ shows a marginal increase in both anodic and cathodic peak currents (Fig. 8(c)). The linear variation could be due to the smaller scan-rates that have been used. The ΔV values (hysteresis between the anodic/cathodic peak voltages) exhibit a significant increase with scan-rate, more so for the 5 wt.% $AlPO_4$-coated compound (Fig. 8(d)). Thus, the CV results demonstrate that ≥5 wt.% $AlPO_4$-coating is able to suppress completely the reversible crystal structure transitions in $Li(Ni_{0.8}Co_{0.2})O_2$ that occur when cycled to >4 V, but causes an increase in the electrode polarization. The mechanism by which the H1 ↔ M, M ↔ H2 and H2 ↔ H3 crystal transitions are suppressed by the $AlPO_4$-coating is not clear at present. Possibly, the Al ions doped into the surface layers of the host compound are responsible for the suppression.

3.3.2. Galvanostatic cycling

Charge–discharge cycling of the cells containing bare, 1, 3, 5 and 8 wt.% $AlPO_4$-coated $Li(Ni_{0.8}Co_{0.2})O_2$ cathodes was continued up to 70 cycles at room temperature and a current density of 30 mA g^{-1} in the voltage range 2.5–4.3 V versus Li. The voltage versus capacity profiles are shown in Fig. 9. On starting the charging process the open-circuit voltage (OCV = 3.1 V) suddenly increases to 3.5 V and then gradually to 4.3 V. The first-charge capacity is 216 mAh g^{-1}, which almost corresponds to the theoretical value of 219 mAh g^{-1} assuming that all the Ni^{3+} ions present in the compound

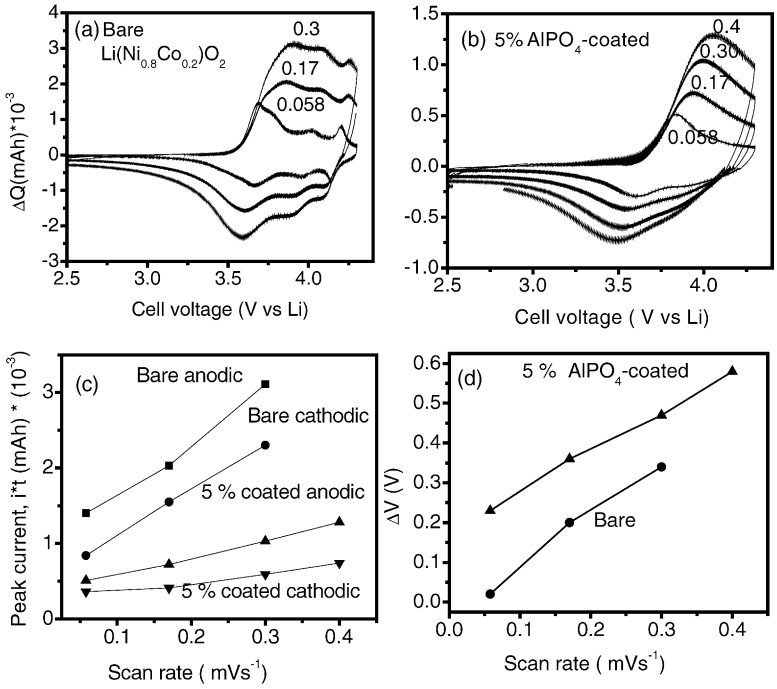

Fig. 8. Cyclic voltammograms of (a) bare and (b) 5 wt.% $AlPO_4$-coated $Li(Ni_{0.8}Co_{0.2})O_2$. Number refers to scan rate, mV s^{-1}. (c) ΔQ ($i \times$ time) vs. scan rate for bare and 5 wt.% $AlPO_4$-coated compound. Anodic and cathodic ΔQ values are indicated. (d) ΔV, difference between anodic and cathodic peak voltages vs. scan rate for bare and 5 wt.% $AlPO_4$-coated compound.

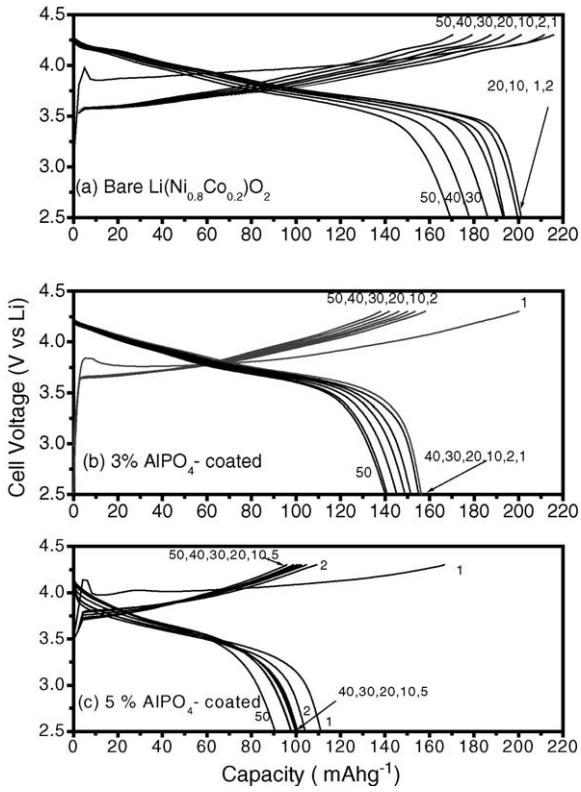

Fig. 9. Voltage vs. capacity profiles at room temperature for (a) bare, (b) 3 wt.% $AlPO_4$-coated and (c) 5 wt.% $AlPO_4$-coated $Li(Ni_{0.8}Co_{0.2})O_2$ between 2.5 and 4.3 V vs. Li-metal at constant current 30 m Ag^{-1}. The numbers refer to cycle numbers.

are oxidized to Ni^{4+} following the extraction of Li from the lattice of $Li(Ni_{0.8}Co_{0.2})O_2$. The first discharge capacity is 194 mAh g^{-1} and hence the irreversible capacity loss (ICL) in the first cycle is 22 mAh g^{-1}. As observed in the CV data, the first cycle is the 'formation' cycle and the ICL arises due to the oxidation of the Ni^{2+} ions present in the Li-layer in the compound during synthesis. In the second and subsequent cycles, these Ni^{3+} ions do not participate in the charge–discharge process, because they get trapped in the Li-layer in accordance with the arguments reported in the literature [16]. After the first few cycles, the observed charge and discharge capacities agree very well and the coulombic efficiency is >98%. The capacity versus number of cycle plots are shown in Fig. 10. It is clear from Figs. 9(a) and 10(a) that the bare compound suffers capacity-fading between 10 and 70 cycles. The 10th cycle capacity of 201(±3) mAh g^{-1} decreases to 159(±3) mAh g^{-1} at the 70th cycle, which corresponds to a capacity-fade of 21%. Similar observations have been made in the literature, and the capacity-fading is attributed to reversible structural transitions in $Li(Ni_{0.8}Co_{0.2})O_2$ [18,20,24,28,34]. Minor changes in the unit-cell volumes that occur during cycling produce 'electrochemical grinding' of the cathode particles and this leads to gradual loss of electrical contact with the other particles and the current-collector.

Galvanostatic curves for 3 and 5 wt.% $AlPO_4$-coated $Li(Ni_{0.8}Co_{0.2})O_2$ are presented in Fig. 9(b) and (c). The capacity versus cycle number plots for these and 1 and 8 wt.% $AlPO_4$-coated compounds are given in Fig. 10(a). The cathodic performance of the 1 wt.% $AlPO_4$-coated compound

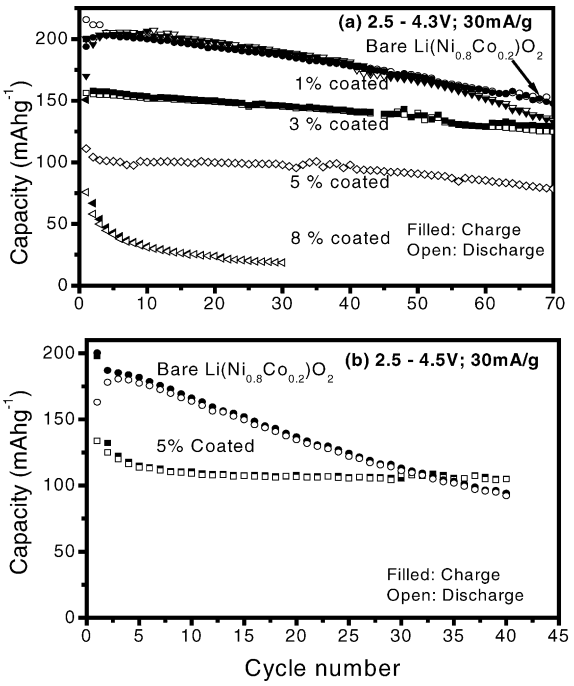

Fig. 10. Capacity vs. cycle number of bare and $AlPO_4$-coated $Li(Ni_{0.8}Co_{0.2})O_2$ at current rate of 30 mA g^{-1}: (a) range 2.5–4.3 V; (b) range 2.5–4.5 V. Filled symbols are for charge, while open symbols are for discharge capacities.

is almost identical to that of bare $Li(Ni_{0.8}Co_{0.2})O_2$ and it is concluded that such a low amount of $AlPO_4$ does not have any influence. A clear influence of coating is experienced for concentrations ≥ 3 wt.% $AlPO_4$. The first charge capacity decreases and the ICL increases with increasing amounts of coated $AlPO_4$. The respective values are—3 wt.% $AlPO_4$: 201 and 43 mAh g^{-1}; 5 wt.%: 167 and 55 mAh g^{-1}; 8 wt.%: 150 and 75 mAh g^{-1}. The reversible capacities, which stabilize after a few initial cycles, exhibit good coulombic efficiency. Nevertheless, the absolute values decrease with increase in the amount of coated $AlPO_4$. The 10th cycle discharge capacities are—3 wt.% $AlPO_4$: 152 mAh g^{-1}; 5 wt.%: 101 mAh g^{-1}; 8 wt.%: 32($\pm$3 mAh g^{-1}). Capacity-fading in 3 and 5 wt.% $AlPO_4$-coated $Li(Ni_{0.8}Co_{0.2})O_2$ is much less than that shown by the bare compound. In the range 10–70 cycles, the capacity-fade for the 3 wt.%-coated compound is ~9%. In the case of the 5 wt.%-coated compound, the reversible capacity of 101 mAh g^{-1} remains stable in the range 10–40 cycles, after which it degrades by ~20% at the 70th cycle. The cathodic performance of the 8 wt.%-coated compound is very poor; the reversible capacity is only 20 mAh g^{-1} after 30 cycles, see Fig. 10(a). It is concluded that 3 wt.% $AlPO_4$-coating is most effective in giving reasonably high capacities and reduced capacity-fading in comparison with bare $Li(Ni_{0.8}Co_{0.2})O_2$ when cycled in the voltage range 2.5–4.3 V up to 70 cycles.

Bare and 5 wt.% $AlPO_4$-coated $Li(Ni_{0.8}Co_{0.2})O_2$ have also been cycled in the voltage range 2.5–4.5 V at 30 mA g^{-1} up to 40 cycles. The capacity versus cycle number plots are given in Fig. 10(b). The higher cut-off voltage causes severe capacity-fading in the bare compound from the second cycle onwards; the 5th cycle charge capacity of 181 mAh g^{-1} falls to 94 mAh g^{-1} at the end of the 40th cycle, which corresponds to 48% fading. This is more than twice the value observed with the 4.3 V cut-off. By contrast, the 5 wt.% $AlPO_4$-coated $Li(Ni_{0.8}Co_{0.2})O_2$ performs well, and is similar to that with a 4.3 V cut-off. The first charge and discharge capacities are 198 and 134 mAh g^{-1}, respectively. These values decrease during 2–10 cycles but stabilize at 110($\pm$5) mAh g^{-1} during 10–40 cycles. As can be seen from Fig. 10(b), the coulombic efficiencies are also good.

The XRD patterns of selected cycled electrodes, in the charged and discharged states, have been recorded after dismantling the cells in a glove-box and recovering the composite electrodes (along with the Al-foil). These ex situ XRD patterns are similar to the virgin (bare or coated) compounds. But a slight broadening of the peaks is observed. The lattice parameters are given in Table 1 and indicate that the crystal structure is stable to cycling. As can be expected, the *a* parameter decreases and *c* and the *c*/*a* parameters increase in the charged state for both the bare and $AlPO_4$-coated compounds. Similar behaviour has been observed [14] for charged $Li(Ni_{0.8}Co_{0.2})O_2$ electrodes, as well as for other cathodes such as $LiNi_xMg_yO_2$[57], $Li(Ni_{0.70}Co_{1.5}Al_{0.15})O_2$[58], and $Li(Ni_{1/3}Co_{1/3}Mn_{1/3})O_2$ [59]. The expansion of the *c* parameter up to 14.44 Å is due to electrostatic repulsion of the oxide ion layers that is caused by the removal of Li ions from Li-layer and the formation of Ni^{4+} (or Co^{4+}) ions in the (NiCo)-layer. The decrease in *R* value from 0.82 ± 0.03 in the virgin state to 0.61 ± 0.01 in the charged state for the 3 and 5 wt.% $AlPO_4$-coated $Li(Ni_{0.8}Co_{0.2})O_2$ (Table 1) shows that some of the Ni-ions have migrated to the Li-layer during cycling and may have contributed to the observed capacity-fading beyond 40 cycles (Fig. 10).

3.3.3. Impedance spectroscopy

Electrochemical impedance spectroscopy (EIS) is a well-adapted technique to reveal the surface film formation during charge–discharge cycling of the cathodes, the processes that occur in the active material of the composite electrode, and the Li ion diffusional processes in the surface film and in the bulk of the oxide. EIS studies have been reported for bare $Li(Ni_{0.8}Co_{0.2})O_2$ [25,34,60], a TiO_2-coated compound [34] and other cathodes such as $LiCoO_2$ [61,62], $LiNiO_2$ [62], $Li(Ni_{1/2}Mn_{1/2})O_2$ [63] and $LiMn_2O_4$ [54,64]. In this work, preliminary measurements have been made at room temperature on cells with 1 and 5 wt.% $AlPO_4$-coated $Li(Ni_{0.8}Co_{0.2})O_2$. The cells were aged for 24 h and were scanned between 2.5 and 4.3 V at 0.058 mV s^{-1} using CV set-up. After the desired number of cycles, the cells were relaxed for 3 h in the charged state and impedance responses were measured, together with those for uncycled cells. The Nyquist plots Z' versus $-Z''$ for the 1 and 5 wt.% $AlPO_4$-coated samples are shown in Fig. 11. A fresh cell with 1 wt.% $AlPO_4$-coated $Li(Ni_{0.8}Co_{0.2})O_2$ as cathode and with an OCV

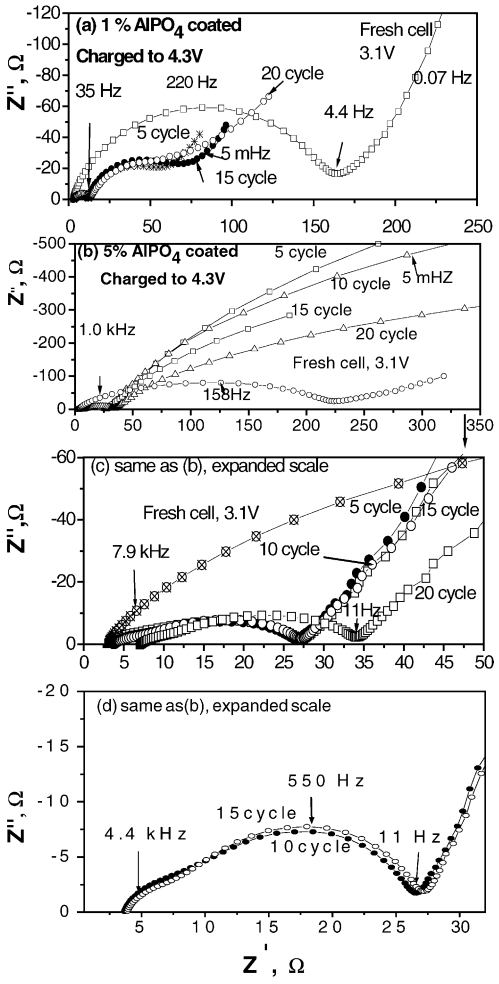

Fig. 11. Nyquist plots (Z' vs. $-Z''$) of the fresh cells and cells in charged state: (a) 1 wt.%; (b) 5 wt.% $AlPO_4$-coated $Li(Ni_{0.8}Co_{0.2})O_2$. Cells were cycled at scan rate of 0.058 mV s^{-1} between 2.5 and 4.3 V and then charged to 4.3 V. Cycle numbers and select frequency values are shown. (c) and (d): same as (b) in expanded scale.

of 3.1 V gives a single semicircle in the high-frequency region (>220 Hz) that intersects the Z′ axis, after curve-fitting, at $157 \pm 3\,\Omega$, followed by Warburg-type behaviour (straight line with 45° angle to the Z' axis) in the low-frequency region (4.4–0.07 Hz). The depressed semicircle is due to the non-homogeneity of the composite electrode. A qualitative change occurs in the impedance spectrum of the cell in the charged state (4.3 V) after five cycles, namely, a well-defined semicircle in the high-frequency region (>0.5 kHz) that, on closer inspection, reveals two overlapping semicircles. A depressed semicircle is shown in the intermediate frequency region (>2 Hz) and a Warburg-region in the low-frequency region (<0.17 Hz). The shape of the spectra remain almost unchanged for the cells after 15 and 20 cycles (Fig. 11(a)).

Similar behaviour is shown by the cells with 5 wt.% $AlPO_4$-coated $Li(Ni_{0.8}Co_{0.2})O_2$. Fresh cell (OCV = 3.1 V) shows a single semicircle with an impedance, after curve-fitting, of $210 \pm 3\,\Omega$ (frequency of 158 Hz at the Z'' maximum), but the Warburg-type sloping region below 4 Hz is absent (Fig. 11(b)). A qualitative change in the impedance spectrum is seen, in the charged state, after five cycles, viz., two overlapping semicircles in the high-to-intermediate frequency range (4.4–0.55 kHz), clearly seen in the expanded scale in Fig. 11(c), and an incomplete semicircle in the low-frequency region (<11 Hz). The Warburg region is absent. The spectra remain mostly unaffected after 10, 15 and 20 cycles (Fig. 11(b–d)). Nobili et al. [25] and Levi et al. [60] have studied the impedance behaviour of cells with $Li_x(Ni_{0.8}Co_{0.2})O_2$ as the cathode and Li-metal as the anode at various voltages (x varying from 1.0 to 0.5). They analyzed the observed data by fitting to equivalent electrical circuits representing R (resistance), capacitance C (or constant phase element, CPE in the case of depressed semicircle), and the Warburg element. In fresh cells, the impedance corresponding to the high-frequency semicircle is generally attributed to the passivating surface-film (solid electrolyte interface, SEI) that forms on the cathode (R_{sf}). In charged or cycled cells, the R_{sf} becomes very much reduced due to the 'formation' cycle, and remains unchanged in subsequent cycles. The impedance of semicircles in the intermediate-frequency (4.0–0.5 kHz) and low-frequency (<11 Hz) ranges is attributed to the bulk resistance (R_b) and charge-transfer (electrolyte–electrode) resistance (R_{ct}) of the cathode, respectively [60]. Nobili et al. [25] have however, argued that the low-frequency impedance corresponds to the bulk resistance (R_b). The Warburg-region is exhibited at very low frequencies ($\ll$1 Hz) and is associated with the Li-ion diffusion process in the cathode. Often, the Warburg-region can be missed either due to the limitation in the measured frequency range or due to masking by the charge-transfer/bulk resistance contributions.

The impedance spectra of 1 and 5 wt.% $AlPO_4$-coated $Li(Ni_{0.8}Co_{0.2})O_2$ in Fig. 11 are qualitatively similar to those reported for $Li(Ni_{0.8}Co_{0.2})O_2$ [25,34,60]. We have fitted the observed spectra to the equivalent electrical circuits representing R_{sf}, R_{ct} and R_b and the respective CPEs (C_{sf}, C_{dl} and C_b) with or without the Warburg element [25,60,63,64]. The parameter C_{dl} represents the double-layer capacitance associated with R_{ct}. Fresh cells show an R_{sf} of 157 and 210 Ω, respectively, for the 1 and 5 wt.% $AlPO_4$-coated compounds. After five cycles, in the charged state, the R_{sf} become small, i.e., 1.5 ± 0.5 and $3 \pm 1\,\Omega$ respectively, for 1 and 5 wt.% $AlPO_4$-coated compounds, and remain constant for ≥10 cycles. The R_b values for 1 wt.% $AlPO_4$-coated compound after ≥5 cycles are $8 \pm 2\,\Omega$, whereas those for 5 wt.% $AlPO_4$-coated compound are larger, by a factor of three ($24 \pm 2\,\Omega$). It is well-known that the bulk resistivity of $Li_x(Ni_{0.8}Co_{0.2})O_2$ in the charged state ($x \sim 0.5$) is smaller by two–three orders of magnitude compared with the fresh or discharged state of the material [14,25]. Hence, the observed R_b values are in order. The R_{ct} values for 1 wt.% $AlPO_4$-coated compound show an increasing trend with increase in the number of cycles, viz., from $48 \pm 2\,\Omega$ after 5 cycles to $64 \pm 2\,\Omega$ after 20 cycles. This can be understood from the fact that 'electrochemical grinding' occurs in the compound on cycling due to reversible phase transitions, and must be one of the reasons for the ob-

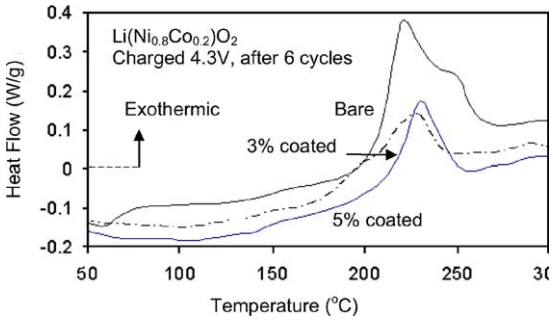

Fig. 12. DSC curves of charged cathodes from cells charged to 4.3 V after six galvanostatic cycles for the bare and $AlPO_4$-coated $Li(Ni_{0.8}Co_{0.2})O_2$. Heating rate, 5 °C min^{-1}.

served capacity-fading (Fig. 10(a)). On the other hand, the R_{ct} values for the 5 wt.% $AlPO_4$-coated compound are very large, i.e., $2390 \pm 5\,\Omega$ after 5 cycles, and decrease with increase in cycle number, finally reaching $860 \pm 5\,\Omega$ after 20 cycles. Since $AlPO_4$ is an electronic insulator, it is expected that ≥5 wt.% coating must give rise to an increase in the charge-transfer resistance. The reasons for the continuous decrease of R_{ct} with the increase in number of cycles with the 5 wt.% $AlPO_4$-coated compound is not clear at present, although it is known that the phase transitions are more or less completely suppressed. The C_{sf}, C_b and C_{dl} values are in the range 130 ± 10 μF, 60–160 μF and 25 ± 5 mF, respectively, and do not show much variation in the 1 and 5 wt.% $AlPO_4$-coated compounds for ≥5 cycles. These values are in the range observed by others on oxide cathodes. Since the cathodic performance of 1 wt.% $AlPO_4$-coated $Li(Ni_{0.8}Co_{0.2})O_2$ is almost the same as that of bare compound, it can be assumed that the impedance response of the former reflects that of the bare compound. Thus, the variation in the impedance parameters for the bare and 5 wt.% $AlPO_4$-coated compounds correlate well with the galvanostatic data. The higher values of R_b and R_{ct} in 5 wt.% $AlPO_4$-coated $Li(Ni_{0.8}Co_{0.2})O_2$ are responsible for the lower reversible capacities in comparison with the bare compound. Nevertheless, the constancy of R_b ($24 \pm 2\,\Omega$) and the decreasing value of R_{ct} for >5 cycles ensures a stable capacity for at least 40 cycles (Fig. 10(a)).

3.3.4. Thermal stability of the charged cathodes

The thermal stability of the cathodes in the charged state (cells charged to 4.3 V after six cycles) was evaluated by differential scanning calorimetry (DSC). The DSC traces of bare and 3 and 5 wt.% $AlPO_4$-coated $Li_{1-x}(Ni_{0.8}Co_{0.2})O_2$, $x \geq 0.5$ are shown in Fig. 12. The heat flow values in the *y*-axis have been normalized with respect to the cathode-active mass in the composite electrode. As can be seen, bare $Li_{1-x}(Ni_{0.8}Co_{0.2})O_2$ displays a characteristic exothermic peak with a decomposition temperature (T_d) of 220 ± 2 °C, in very good agreement with the reported values (210–220 °C) [18,22,28]. The heat evolution is due to the decomposition and destruction of the layer structure with the liberation of oxygen. This occurs mainly because of the instability of the Ni^{4+} (and Co^{4+}) ions in the lattice at high temperature. Both the 3 and 5 wt.% $AlPO_4$-coated compounds show a shift towards higher temperature, by ∼10 °C, with $T_d = 230 \pm 2$ °C. Significantly, the integrated relative peak areas for the coated compounds are smaller by a factor of 5 in comparison with the bare $Li_{1-x}(Ni_{0.8}Co_{0.2})O_2$ (Fig. 12). A similar decrease in the heat evolution, by a factor of 10, and enhancement of T_d (by ∼50 °C) have been observed for $AlPO_4$-coated $LiCoO_2$ cathodes when charged to 4.3 V [38]. Hence, it is concluded that $AlPO_4$-coating of $Li(Ni_{0.8}Co_{0.2})O_2$ provides better thermal stability in the charged state.

4. Conclusions

The surface of the particles of the layered oxide, $Li(Ni_{0.8}Co_{0.2})O_2$ have been coated with $AlPO_4$ and their cathodic behaviour has been examined in cells with Li metal as the anode.

The bare (uncoated) compound is synthesized as a crystalline powder by the mixed-hydroxide method at 725 °C in an oxygen atmosphere. It is then coated with $AlPO_4$, from 1 to 8 wt.%, by the solution method and heat-treated at 700 °C in oxygen. All the compounds are characterized by powder XRD, XPS, SEM, EDAX, TEM, BET-surface area and density methods. The XRD analysis shows that the hexagonal *a* and *c* lattice parameters of $Li(Ni_{0.8}Co_{0.2})O_2$ are not affected by the $AlPO_4$-coating, but there are indications of an increasing number of Ni-ions occupying the Li-sites in the Li-layer with increasing amounts of coated $AlPO_4$. The XPS data show that Ni, Co and Al ions are trivalent, as expected. The O 1s spectra clearly indicate two different oxygens that correspond to the coated-$AlPO_4$ and the bare compounds. Micrographs from SEM and TEM studies reveal that $AlPO_4$ is not uniformly coated on $Li(Ni_{0.8}Co_{0.2})O_2$ for compositions ≥5 wt.%. Cyclic voltammetry (CV) of the bare compound shows redox processes at 3.65–3.8 V (versus Li) that correspond to the $Ni^{3+/4+}$ couple and characteristic structural phase transitions at higher voltages. These transitions are suppressed by a ≥5 wt.% $AlPO_4$-coating. Galvanostatic charge–discharge cycling performed at a current density of 30 mA g^{-1} in the range 2.5–4.3 V up to 70 cycles demonstrates that the first cycle capacity loss increases, and the reversible capacities decrease, with an increasing amount of coated $AlPO_4$. After 10 cycles, for example the discharge capacities are—bare $Li(Ni_{0.8}Co_{0.2})O_2$: 201 mAh g^{-1}; 3 wt.% $AlPO_4$: 152 mAh g^{-1}; 5 wt.%: 101 mAh g^{-1}; 8 wt.%: 32(±3 mAh g^{-1}). Capacity-fading in the 3 and 5 wt.% $AlPO_4$-coated $Li(Ni_{0.8}Co_{0.2})O_2$ is much less than that shown by the bare compound. In the range 10 to 70 cycles, capacity-fade for the bare and 3 wt.% coated compounds is 21 and 15% respectively. In the case of the 5 wt.% coated compound, the reversible capacity of 101 mAh g^{-1} remained stable in the range 10–40 cycles, after which it degraded by ∼20% at the 70th cycle. The coulombic efficiency is

>98% in all cases. The cathodic performance of the 8 wt.% coated compound is very poor. Bare and 5 wt.% $AlPO_4$-coated compounds have also been cycled between 2.5 and 4.5 V at 30 mA g^{-1} up to 40 cycles. The fifth cycle charge capacity of 181 mAh g^{-1} for the bare compound decreased to 94 mAh g^{-1} after 40 cycles, which corresponds to 48% capacity-fading. The 5 wt.% $AlPO_4$-coated compound displays a stable capacity of 110 ± 5 mAh g^{-1} between 10 and 40 cycles. Ex situ XRD of 3 and 5 wt.% $AlPO_4$-coated, charged cathodes (to 4.3 V after 70 cycles) reveals that the crystal structure is stable to cycling but indicates that increasing amounts of Ni-ions occupy the Li-layer. Impedance studies of uncycled and cycled cells (charged state, to 4.3 V) exhibit the beneficial effect of 5 wt.% $AlPO_4$-coating of $Li(Ni_{0.8}Co_{0.2})O_2$ in that the deduced values of R_b and R_{ct} are larger than those of 1 wt.% $AlPO_4$-coated compound, but help to suppress capacity-fading in the range 10–40 cycles. The DSC curves of the charged cathodes, 4.3 V after six cycles, reveal that the decomposition temperature (T_d) of 220 °C for the bare compound increased by ~10 °C after 3 and 5 wt.% $AlPO_4$-coating, and more significantly, the heat evolution decreases by a factor of 5. This concluded that a ≥3 wt.% $AlPO_4$-coating of $Li(Ni_{0.8}Co_{0.2})O_2$ is effective in reducing capacity-fading and increasing its thermal stability in the charged state. These benefits come, however at the expense of reversible capacity, which decreases from 202 mAh g^{-1} for the bare compound on the fifth cycle, to 156 and 100 mAh g^{-1} (2.5–4.3 V) for the 3 and 5 wt.% $AlPO_4$-coated samples respectively.

Acknowledgements

Thanks are due to Dr. S. Madhavi, NTU, Singapore, for help with the EDAX measurements and Mdm. Leng Lee Eng, Dept. of Chemistry, NUS for assistance with the DSC studies.

References

[1] J.-M. Tarascon, M. Armand, Nature 414 (2001) 359.
[2] M. Wakihara, Mater. Sci. Eng. R33 (2001) 109.
[3] W.A. Van Schalkwijk, B. Scrosati (Eds.), Advances in Lithium-ion Batteries, Kluwer Academic Publishers/Plenum Press, New York, USA, 2002.
[4] W. Li, J.N. Reimers, J.R. Dahn, Solid State Ion. 67 (1993) 123.
[5] H. Arai, S. Okada, Y. Sakurai, J.I. Yamaki, Solid State Ion. 95 (1997) 275.
[6] T. Ohzuku, Y. Makimura, Chem. Lett. (Jpn.) (2001) 744.
[7] Z. Lu, J.R. Dahn, J. Electrochem. Soc. 149 (2002) A815.
[8] K.M. Shaju, G.V. Subba Rao, B.V.R. Chowdari, Electrochim. Acta 48 (2003) 1505.
[9] G. Amatucci, J.-M. Tarascon, J. Electrochem. Soc. 149 (2002) K31.
[10] C. Delmas, I. Saadoune, A. Rougier, J. Power Sources 44 (1993) 595.
[11] A. Rougier, I. Saadoune, P. Gravereau, P. Willmann, C. Delmas, Solid State Ion. 90 (1996) 83.
[12] H. Arai, S. Okada, Y. Sakurai, J.-I. Yamaki, J. Electrochem Soc. 144 (1997) 3117.
[13] M. Okada, K.-I. Takahashi, T. Mouri, J. Power Sources 68 (1997) 545.
[14] I. Saadoune, C. Delmas, J. Solid State Chem. 136 (1998) 8.
[15] R.K.B. Gover, M. Yonemura, A. Hirano, R. Kanno, Y. Kawamoto, C. Murphy, B.J. Mitchell, J.W. Richardson Jr., J. Power Sources 81-82 (1999) 535.
[16] C. Delmas, M. Ménétrier, L. Croguennec, S. Levasseur, J.P. Pérès, C. Poullerie, G. Pradao, L. Fournès, F. Weill, Int. J. Inorg. Mater. 1 (1999) 11.
[17] J. Cho, G. Kim, H.S. Lim, J. Electrochem. Soc. 146 (1999) 3571.
[18] J. Cho, H.-S. Jung, Y.-C. Park, G.-B. Kim, H.-S. Lim, J. Electrochem. Soc. 147 (2000) 15.
[19] R.K.B. Gover, R. Kanno, B.J. Mitchell, M. Yonemura, Y. Kawamoto, J. Electrochem. Soc. 147 (2000) 4045.
[20] K.-K. Lee, K.-B. Kim, J. Electrochem. Soc. 147 (2000) 1709.
[21] R. Gover, R. Kanno, B. Mitchell, A. Hirano, Y. Kawamoto, J. Power Sources 90 (2000) 82.
[22] R. Venkatachalapathy, C.W. Lee, W.Q. Lu, J. Prakash, Electrochem. Commun. 2 (2000) 104.
[23] W. Lu, C.W. Lee, R. Venkatachalapathy, J. Prakash, J. Appl. Electrochem. 30 (2000) 1119.
[24] E. Levi, M.D. Levi, G. Salitra, D. Aurbach, R. Oesten, U. Heider, L. Heider, Solid State Ion. 126 (1999) 97.
[25] F. Nobili, F. Croce, B. Scrosati, R. Marassi, Chem. Mater. 13 (2001) 1642.
[26] J. Yang, C. Wan, C. Jiang, Y. Li, J. Power Sources 99 (2001) 78.
[27] R.K.B. Gover, R. Kanno, B.J. Mitchell, A. Hirano, Y. Kawamoto, J. Power Sources 97/98 (2001) 316.
[28] B.V.R. Chowdari, G.V. Subba Rao, S.Y. Chow, Solid State Ion. 140 (2001) 55.
[29] C.-H. Lu, H.-C. Wang, J. Mater. Chem. 13 (2003) 428.
[30] S. Venkatraman, Y. Shin, A. Manthiram, Electrochem. Solid-State Lett. 6 (2003) A9.
[31] H.-J. Kweon, S.J. Kim, D.G. Park, J. Power Sources 88 (2000) 255.
[32] B.V.R. Chowdari, G.V. Subba Rao, S.Y. Chow, J. Solid State Electrochem. 6 (2002) 565.
[33] Z.R. Zhang, H.S. Liu, Z.L. Gong, Y. Yang, J. Electrochem. Soc. 151 (2004) A599.
[34] Z.R. Zhang, H.S. Liu, Z.L. Gong, Y. Yang, J. Power Sources 129 (2004) 101.
[35] H. Omada, T. Brousse, C. Marhic, D.M. Schleich, J. Electrochem. Soc. 151 (2004) A922.
[36] J. Cho, Y.-W. Kim, B. Kim, J.-G. Lee, B. Park, Angew. Chem. Intl. Ed. 42 (2003) 1618.
[37] J. Cho, Electrochem. Commun. 5 (2003) 146.
[38] J. Cho, J.-G. Lee, B. Kim, B. Park, Chem. Mater. 15 (2003) 3190.
[39] J. Cho, J. Power Sources 126 (2004) 186.
[40] B. Kim, J.-G. Lee, M. Choi, J. Cho, B. Park, J. Power Sources 126 (2004) 190.
[41] K.M. Shaju, G.V. Subba Rao, B.V.R. Chowdari, Electrochim. Acta 48 (2002) 145.
[42] R.D. Shannon, Acta Crystallogr. Sect. A 32 (1976) 751.
[43] J.F. Moulder, W.F. Stickle, P.E. Sobol, I.L.D. Bomben, in: J. Chastain, R.C. King Jr. (Eds.), Handbook of X-ray Photoelectron Spectroscopy, Physical Electronics Inc., Minnesota, 1995.
[44] M.E. Spahr, P. Novak, B. Schnyder, O. Haas, R. Nesper, J. Electrochem. Soc. 145 (1998) 1113.
[45] V.R. Galakhov, E.Z. Kurmaev, S. Uhlenbrock, M. Neumann, D.G. Kellerman, V.S. Gorshkov, Solid State Commun. 99 (1996) 221.
[46] A.F. Carley, S.D. Jackson, J.N. O'Shea, M.W. Roberts, Surf. Sci. 440 (3) (1999) L868.
[47] K. Amine, H. Tukamoto, H. Yasuda, Y. Fujita, J. Electrochem. Soc. 143 (1996) 1607.
[48] A.N. Mansour, Surf. Sci. Spectra 3 (1996) 279.
[49] K.M. Shaju, G.V. Subba Rao, B.V.R. Chowdari, Solid State Ion. 152–153 (2002) 69.

[50] K.M. Shaju, K.V. Ramanujachary, S.E. Lofland, G.V. Subba Rao, B.V.R. Chowdari, J. Mater. Chem. 13 (2003) 2633.
[51] J.A. Rotole, P.M.A. Sherwood, Surf. Sci. Spectra 5 (1998) 60.
[52] W. Li, J.N. Reimers, J.R. Dahn, Solid State Ion. 67 (1993) 123.
[53] S. Madhavi, G.V. Subba Rao, B.V.R. Chowdari, S.F.Y. Li, J. Power Sources 93 (2001) 156.
[54] K.A. Striebel, A. Rougier, C.R. Horne, R.P. Reade, E.J. Cairns, J. Electrochem. Soc. 146 (1999) 4339.
[55] M. Morcrette, P. Barboux, J. Perrière, T. Borusse, A. Traverse, J.P. Boilot, Solid State Ion. 138 (2001) 213.
[56] S.-I. Pyun, H.-C. Shin, J. Power Sources 97/98 (2001) 277.
[57] C. Pouillerie, L. Croguennec, C. Delmas, Solid State Ion. 132 (2000) 15.
[58] M. Guilmard, C. Pouillerie, L. Croguennec, C. Delmas, Solid State Ion. 160 (2003) 39.
[59] D.-C. Li, T. Muta, L.-Q. Zhang, M. Yoshio, H. Noguchi, J. Power Sources 132 (2004) 150.
[60] M.D. Levi, K. Gamolsky, D. Aurbach, U. Heider, R. Oesten, Electrochim. Acta 45 (2000) 1781.
[61] Y.-M. Choi, S.-I. Pyun, Solid State Ion. 99 (1997) 173.
[62] Y.-M. Choi, S.-I. Pyun, J.-S. Bae, S.-I. Moon, J. Power Sources 56 (1995) 25.
[63] K.M. Shaju, G.V. Subba Rao, B.V.R. Chowdari, Electrochim. Acta 49 (2004) 1565.
[64] K.M. Shaju, G.V. Subba Rao, B.V.R. Chowdari, J. Mater. Chem. 13 (2003) 106.